Revision 1

The role of water in generation of group II kimberlite magmas: constraints from multiple saturation experiments

Alexander G. Sokol[1,2]*, Alexey N. Kruk[1] and Yury N. Palyanov[1,2]

[1] V.S. Sobolev Institute of Geology and Mineralogy, Russian Academy of Sciences, Siberian Branch, 3, Koptyug Ave., Novosibirsk, 630090, Russian Federation
[2] Novosibirsk State University, 2, Pirogov str., Novosibirsk, 630090, Russian Federation

*Corresponding author. E-mail address: sokola@igm.nsc.ru

ABSTRACT

Multiple saturation experiments have been performed in a multicomponent system at 6.3 to 7.5 GPa and 1400-1670°C using a split-sphere multianvil apparatus to constrain the conditions of kimberlite magma generation. The starting bulk compositions of samples corresponded to the average group II kimberlite (orangeite), with water contents varying from 5 to 9 wt.% H_2O and the $CO_2/(CO_2+H_2O)$ molar ratio from 0.37 to 0.24. The charges were placed inside graphite liners sealed in Pt capsules to avoid Fe loss. Oxygen fugacity (fO_2) during the experiment was buffered by the equilibrium between graphite and a hydrous carbonate-silicate melt about EMOG/D. As water in the starting kimberlite increased from 5 to 9 wt.%, the temperature of its complete melting became ~100°C lower (relative to 1670°

C), both in the 6.3 GPa and 7.5 GPa runs. Orthopyroxene was stable just below the liquidus at all pressures and H_2O concentrations applied in the experiments. An olivine + garnet + orthopyroxene assemblage was present at ≤100°C below the liquidus when H_2O was 5 wt.%. At 7 and 9 wt.% H_2O, the same assemblage appeared at 100-150°C and >200°C below the liquidus, respectively. In no experiment was clinopyroxene observed as a run product. Olivine, garnet, and orthopyroxene stable in the multiply saturated melt were compositionally similar to mantle peridotite minerals found as xenoliths in kimberlites worldwide. Thus we infer that generation of group II kimberlite magma may occur by partial melting of carbonated (metasomatized) garnet harzburgite at pressures from 6.3 to 7.5 GPa, temperatures about 1500-1600°C, and no more than 5 wt.% H_2O in the melt. Water, in the amounts required to produce this magma, may come from interaction of K-Ca-rich carbonatite melt, infiltrating from a deeper mantle source, with a peridotite protolith containing H_2O in nominally anhydrous minerals and, possibly, also in phlogopite.

Keywords: experiment, mantle, kimberlite, magma, water, fluid

INTRODUCTION

Group II (micaceous) kimberlite is an ultrabasic rock rich in potassium and volatiles, with macrocrysts and phenocrysts of phlogopite in the groundmass (Smith et al. 1985; Mitchell 1986). Its geochemistry indicates an origin from lithospheric mantle source regions metasomatized by melts or fluids associated with ancient subduction events (Becker and Le Roex 2006). However, the specific conditions of magma generation, and especially the role

of volatiles, remain a subject of discussions (Ulmer and Sweeney 2002; Brey et al. 2008; 2009; Foley et al. 2009; Kamenetsky et al. 2009; Girnis et al., 2011; Sokol et al. 2013a,b). According to experimental evidence, kimberlite magma can be produced by small-degree partial melting of carbonated peridotite in lower lithospheric or asthenospheric sources (Canil and Scarfe 1990; Gudfinnsson and Presnall 2000; Ulmer and Sweeney 2002; Brey et al. 2008; 2009; Foley et al. 2009). Strongly fractionated REE patterns of kimberlites, with high LREE enrichment, imply partial melting in the presence of residual garnet (Mitchell 1986; Ringwood et al. 1992). Thus, olivine, garnet and pyroxene should be present at or near the liquidus in kimberlite magmas in the P, T, fH_2O and fCO_2 conditions in which they separated from their source lithology (Ringwood et al. 1992).

The pressures and temperatures at which magma becomes saturated in near-liquidus multiphase residue can be found experimentally by the so-called multiple saturation technique. It is applicable if (1) the starting material represents a primary magma composition; (2) equilibrium is achieved between the melt phase and the residue at a specific pressure and temperature (Ulmer and Sweeney 2002; Funk and Luth 2012).

Saturation of group II kimberlite melt with olivine, orthopyroxene and garnet (garnet harzburgite residue) was studied (Ulmer and Sweeney 2002) at pressures from 4 to 10 GPa and at temperatures in a broad range. Note that the cited experiments at the pressures 6.0 and 7.5 GPa, the most important for group II kimberlite generation, were run at temperatures within 1480°C and 1450°C, respectively, and the liquidus was not encountered. The authors suggested two explanations of their results: either (i) the used kimberlite compositions did not represent the primary compositions being enriched in olivine, orthopyroxene, or garnet components by incorporation of harzburgitic xenoliths, or (ii) the group II kimberlite

compositions represented a liquid, which most likely was in equilibrium with a garnet harzburgite residue (Ulmer and Sweeney 2002).

A later detailed geochemical study of hypabyssal group II kimberlites from South Africa (Becker and Le Roex 2006) allowed estimating the average close-to-primary kimberlite magma composition (the one least affected by alteration, crustal contamination and fractional crystallization, and corrected for macrocryst entrainment) (Table 1). Compared with the close-to-primary kimberlite magma composition from (Becker and Le Roex 2006), the average composition of group II kimberlites used in (Ulmer and Sweeney 2002) contains similar amounts of SiO_2, the latter being slightly more enriched in MgO (29.1 against 23.1 wt.%, respectively) and depleted in CaO (5.9 and 10.0 wt.%, respectively). However, the difference appears to be not very significant taking into account the uncertainty in the estimates of average close-to-primary kimberlite magma composition (Becker and Le Roex 2006). It is more important that the $X_{CO2}=CO_2/(CO_2+H_2O)$ molar ratio (0.19) in this composition (Becker and Le Roex 2006) is much below the 0.37 value in the kimberlite used for the multiple saturation experiments of Ulmer and Sweeney (2002).

The composition and amounts of fluids were shown earlier (Girnis et al. 1995) to strongly affect near-liquidus phase relations in group I kimberlites, and magnesite instead of olivine to become stable close to the liquidus at 5.5 GPa and $X_{CO2}>0.7$. Later we (Sokol et al. 2013a) encounter near-liquidus Ol+Grt+Cpx saturation of the Udachnaya group I kimberlite melt at 6.3 and 7.5 GPa and $X_{CO2}=0.26$-0.38. At the same time, only Ol+Grt appeared near the liquidus in 6.5 GPa experiments with a low-H_2O composition of the Udachnaya kimberlite at X_{CO2} about 0.8 (Sharygin et al. 2013). Note that simultaneous

93 saturation of kimberlite melts of other compositions is possible at a broad range of X_{CO2}
94 conditions (Eggler and Wendlandt 1979; Girnis et al. 2011).

95 Below we report a detailed multiple saturation experimental study of group II
96 kimberlite at the pressures 6.3 and 7.5 GPa corresponding to its generation depths in
97 subcratonic lithospheric mantle. We have constrained the liquidus temperatures for the
98 average composition of group II kimberlites used in (Ulmer and Sweeney 2002) and studied
99 the near-liquidus phase relations in the system at 5 to 9 wt.% bulk H_2O and X_{CO2}=0.24-0.37.
100 The reported results have implications for the potential temperatures of magma generation in
101 subcratonic lithosphere, as well as for the source composition and role of volatiles in the
102 primary magma.
103

104 ## EXPERIMENTAL AND ANALYTICAL PROCEDURES

105

106 ### Starting materials

107

108 The starting bulk kimberlite composition (Table 1) selected to study the P-T conditions
109 and the role of water in magma generation corresponded closely to the average group II
110 kimberlite (Smith et al. 1985) but with slightly higher (0.93 wt.%) Na_2O, as reported in
111 (Ulmer and Sweeney 2002). The composition B_1 we used was identical to A (Table 1), and
112 the compositions B_2, B_3, and B_4 differed from A in the amount of water only. The basic
113 composition was prepared following the procedure from (Ulmer and Sweeney 2002):
114 synthesized from reagent-grade chemicals, previously dried at 1100°C (SiO_2, TiO_2, Cr_2O_3,
115 Al_2O_3, MgO, MnO, NiO), weighed, homogenized in an agate mortar under alcohol, and

fired again at 1100°C. Fe was added as presynthesized fayalite, and carbonate was added as $CaCO_3$, K_2CO_3, Na_2CO_3, and $MgCO_3$. Water was added as $Mg(OH)_2$ to charges of a standard composition with 5 wt.% H_2O; the compositions were homogenized, dried, and stored at 90°C. In the case of 7-9 wt.% H_2O compositions, it was distilled water added by a micro-syringe (± 0.2 mg accuracy), immediately before the final capsule assembly.

The choice of capsule material in long-run high-temperature experiments with volatiles is a challenge because of Fe loss, which typically results from Fe alloying with Pt. Ulmer and Sweeney (2002) used simple Pt capsules without liners at 6.0 to 7.5 GPa and T>1350°C, i.e., in the pressure and temperature ranges of special interest to study the phase composition of group II kimberlite. In those experiments, they reduced the Fe loss to minimum by keeping the run times short (0.1 to 0.5 hour). Inasmuch as Fe loss is known (Brey et al. 2011) to increase fO_2 in samples to about the FMQ buffer, Ulmer and Sweeney (2002) may have studied the high-temperature phase composition of group II kimberlite at fO_2 slightly above the CCO buffer. An alternative way is to use graphite liners sealed in the Pt capsules (Girnis et al. 1995; Ulmer and Sweeney 2002) which minimizes the Fe loss to Pt capsules and, at the same time, buffers fO_2. That was the approach Ulmer and Sweeney (2002) applied in their 8.0-9.5 GPa experiments and the one we chose for our study.

The chosen Pt capsules (6.0 mm OD, 5.5 mm ID, 3.2 mm long) allowed us to perform experiments at T>1400°C, i.e., near the kimberlite liquidus. The graphite liners (with 0.5 mm thick walls) welded into the Pt capsules isolated them from interacting with the kimberlite melt and minimized Fe loss. Buffering by the graphite liners provided a realistic oxygen fugacity in the samples: fO_2 close to or slightly below the EMOG/D buffer

(Stagno and Frost 2010) corresponding to equilibrium between graphite and a carbon-bearing carbonate-silicate melt.

After water addition and final assembling, the Pt capsules were placed inside a vessel filled with liquid nitrogen and welded shut (weight losses after sealing were <0.3 mg). The total error on addition of extra amounts of water was ±0.3 wt.%, as estimated on weighing the sealed capsules. After welding, the capsules were compressed to 0.5 GPa for 2 min using a die mold for the waterproof test to ensure its impermeability. The capsules that failed the waterproof test, judging by moisture appeared on its surface, were discarded. For the 6.3 GPa runs, the Pt capsules were additionally pressed into CsCl. Weighing the recovered Pt capsules before and after piercing clearly demonstrated the presence of fluid in the sample after quenching.

High pressure apparatus

Two series of experiments at 6.3 and 7.5 GPa have been carried out in a split-sphere multianvil high-pressure apparatus (Palyanov et al. 2010). The multianvil sphere of 8/6 type consists of two anvils with square faces on top and bottom and four side anvils with rectangular faces placed in an octahedral cavity formed by truncating the vertices of eight steel anvils. The sizes of the high-pressure cell were 21.1×21.1×25.4 mm and 19×19×22 mm, respectively, in the 6.3 GPa and 7.5 GPa runs; the graphite heaters in the two pressure runs had the inner diameters of 12 mm and 9 mm and the heights 18.8 mm and 14.8 mm respectively. Pressure was calibrated by recording the change in the resistance of Bi at 2.55 GPa and of PbSe at 4.0 and 6.8 GPa at room temperature and by bracketing the graphite-

diamond equilibrium at high temperatures (Kennedy and Kennedy 1976). Temperature was monitored in each experiment with a $PtRh_6/PtRh_{30}$ thermocouple calibrated at 6.3 GPa and 7.5 GPa using the melting points of Ag, Ni and Pt. For details of the pressure and temperature calibration see (Sokol et al. 2007; Palyanov et al. 2010). The pressure and temperature were measured to the accuracy ±0.1 GPa and ±20°C.

Analytical technique

The recovered Pt capsules were cleaned from CsCl, dried, weighed, and then sawed longitudinally into halves producing a full top-to-bottom section. One half was embedded in low-viscosity epoxy resin by vacuum impregnation and polished, without the use of water. Samples were studied using optical and scanning electron (Tescan MYRA 3 LMU) microscopy. Electron microprobe analyses (EMPA) were performed at 20 kV accelerating voltage and a 20 nA beam current on a Cameca Camebax and a Jeol JXA-8100 microanalyzers; the beam diameters for silicate and carbonate phases were 1 to 2 μm. The standards used were: pyrope for Si, Al, and Fe; diopside for Mg and Ca; albite for Na; orthoclase for K; ilmenite for Ti; and spinel for Ni. The uncertainty of the measurements was within 2 relative percent for all components.

In spite of fast cooling rates (150-200°/s), the synthesized melts were not quenched to glass but rather formed aggregates of feather-like phases consisting of 50 to 500 μm dendritic silicate and carbonate crystals (Fig.1). The quenched melts were analyzed by a defocused beam with a scanning area of 100×100 μm at 20 kV accelerating voltage and a 40 nA beam current on a Cameca Camebax and a Jeol JXA-8100 microprobes. However, it was

184 virtually impossible to constrain the exact composition of quenched liquids even with this
185 approach, as it was noted in many publications (e.g., Ulmer and Sweeney 2002). The
186 analyses of bulk melt compositions turned out to have quite large standard deviations,
187 especially in alkalis. For this reason, the EMPA data on alkali concentrations in melts were
188 corrected on the basis of mass-balance constraints.
189
190 **RESULTS**
191
192 **Approach to equilibrium**
193
194 The role of water in the generation of group II kimberlite magma was studied in two
195 series of experiments at pressures 6.3 and 7.5 GPa, with water contents in kimberlite from 5
196 to 9 wt.%. Most of the runs at subliquidus temperatures lasted 40 hours and only four
197 experiments at the liquidus were as short as 1-2 hours. The melt pools and the residual
198 phases apparently arrived at equilibrium at long experimental times, as we may infer from
199 earlier time series experiments in a dry peridotite – CO_2 system conducted under similar P-T
200 conditions (Brey et al. 2008), in which the compositions of both melt and peridotite minerals
201 became time-invariant already after the first few hours at 1500°C. Generally, the low
202 viscosity of H_2O-rich carbonate-silicate melts, high temperatures and long experimental
203 times should be favorable for equilibration. The attainment of equilibrium was judged by the
204 observed homogeneity of melt and crystalline phases. Furthermore the phases crystallized at
205 the boundary with the melt pool had the same composition as those located at some distance
206 off this boundary. Complete melting of kimberlite was achieved in almost all 1-2-hour runs.

Minor amounts of Opx in equilibrium with the liquid were observed only in a single 2-hour run, and almost all Opx grains contacted the liquid, which was expected to provide equilibrium, given that the temperature was as high as 1600°C. Note also that Fe loss from the samples was basically minor and caused no influence on the results due to fO_2 buffering by the graphite.

Phase equlibria

The weight proportions of phases in the experiment products were determined by least-squares mass balance calculation for a restricted number of components in the system: SiO_2, TiO_2, Al_2O_3, MgO, and CaO. The calculations were made using the starting kimberlite and chemical compositions of phases, and were accurate to about the sum of squared residuals ≤1. The results are summarized in Tables 2 and 3, and in Figures 1, 2 and 3.

In the 6.3 GPa experiment runs, complete melting was observed at 1670°C for the 5 wt.% H_2O starting composition (Table 2; Fig. 2a) and at 1570°C for that with 9 wt.% H_2O. Judging by the melt fraction trends and the experimental superliquidus temperatures, the liquidus of kimberlite with 5 wt.% H_2O and 9 wt.% H_2O may be expected at ~1650°C and ~1540°C, respectively. For the entire range of H_2O contents, Opx was the first phase crystallized below the liquidus. At 5 wt.% H_2O, crystallization of olivine and garnet initiated in a narrow temperature interval (Fig. 2a), namely, the temperature gap between the liquidus and the appearance of the olivine+garnet+orthopyroxene assemblage in equilibrium with the liquid was below 100°C (Fig. 1). However, at 7 and 9 wt.% H_2O, the same assemblage appeared at 100-150°C and >200°C below the liquidus, respectively. The assemblage

remained stable in the presence of liquid from 1400°C to 1570°C at 5 wt.% H_2O in kimberlite. Therefore, near-liquidus multiple saturation was achieved at 5 wt.% H_2O but was absent in the case of more hydrous compositions of kimberlite.

At 7.5 GPa and water contents of 5 and 9 wt.%, complete melting of kimberlite was detected at 1670°C and 1600°C, respectively. Analysis of the trends (Table 2, Fig. 2b) and conditions of superliquidus experiments suggests that the liquidus for kimberlite with 5 wt.% H_2O and 9 wt.% H_2O should correspond to ~1680°C and ~1580°C, respectively. Orthopyroxene remained the only near-liquidus solid phase. The estimated temperatures of the onset of crystallization for olivine and garnet are given in Fig. 2b. The olivine+garnet+orthopyroxene assemblage in equilibrium with the melt likewise appeared below a gap of <100°C at 5 wt.% H_2O and remained stable within the temperature range from 1500 to 1570°C. However, the high temperature limit of the assemblage stability decreased dramatically at water contents above 5 wt.%. Thus, the near-liquidus multiple saturation was restricted to the composition with 5 wt.% H_2O.

In two experiment runs (# 1350, at 6.3 and 1570 °C and # 1621-1, at 7.5 GPa and 1570°C), we observed graphite-to-diamond conversion in graphite liners with samples bearing 5 wt.% H_2O. This led to underestimation of the melt fractions because some liquid became consumed on percolation between the newly formed diamond aggregates. Investigating these processes, including diamond formation, is however beyond the scope of this paper and is expected to be a subject of a special further study.

Compositions of liquid and solid phases

253 The composition of quench liquids depends on the melting degree, which, in turn, is a
254 function of temperature and water content in the system. At 1400-1470°C and 5 wt.% H_2O,
255 the melting degree was under 50 wt.%, and the melt formed a separate pool, slightly more
256 than one third of the sample, in the high-temperature region of the capsule (Table 2). The
257 melt had a carbonate-silicate composition (SiO_2 15-25 wt.%) and was rich in alkalis (4.2
258 wt.% K_2O), with CaO# from 0.22 to 0.33 (Table 3; Fig. 3a, b, e). As the temperature
259 increased, the main compositional trends of the liquid were to increase in SiO_2 and MgO and
260 to decrease in CaO (Fig. 3). SiO_2 approached 30 wt.% only at >1600°C at 5 wt.% H_2O, both
261 in the 6.3 and 7.5 GPa runs. The melt contained more silica in the case of 7-9 wt.% H_2O in
262 kimberlite than with that of 5 wt.% H_2O, at the same temperatures, due to a greater melting
263 degree of the more hydrous samples. The Ca number in the melt of kimberlite with 5 wt.%
264 H_2O decreased from 0.3 to approximately 0.12 as the temperature changed from 1400°C to
265 1610°C (Fig. 3e), which generally corresponds to the trend in the melts of dry carbonated
266 peridotite (Brey et al. 2009; Stagno and Frost 2010). However, in the case of ≥6 wt.% H_2O,
267 Ca# of the melts became <0.2 already at 1450°C, this being consistent with low Ca# of
268 melts derived from hydrous carbonated peridotite reported by Foley et al. (2009). Note that
269 Al_2O_3 in the melt was close to 3 wt.% and depended neither on temperature nor on water
270 content in the charge (Fig. 3c, d). The obtained kimberlite liquids had the ratios of Al and
271 divalent cations similar to those in the primary magma of group II kimberlite (Fig. 3f)
272 (Becker and Le Roex 2006).
273 The graphite-to-diamond conversion in the graphite liner during the long high-
274 temperature runs # 1350 and # 1621-1 affected the kimberlite melt fraction and even melt
275 composition. To check the effect of diamond synthesis in the graphite liners on the

composition of melt forming immediately below the liquidus, another experimental run was performed at 6.3 GPa and 1610°C (#1667). It was 1.5 hours long, i.e., far shorter than the induction time required for diamond nucleation (Palyanov and Sokol, 2009). Indeed, SiO_2 and MgO in the melt decreased while CaO increased as a result of diamond synthesis (point "G-D" in Fig. 3).

Neither sample produced in this study showed fluid phase bubbles. Thus, no free fluid segregation occurred within the studied range of water concentrations, the water solubility in the kimberlite melt exceeded 9 wt.%, and the melt remained unsaturated with respect to water.

Olivine occurred as subhedral, sometimes prismatic, crystals from 30 μm at low temperatures up to 500 μm at 1500-1570°C. The small crystals were colorless while the large ones had a greenish hue (Fig. 1). Olivine in the samples with 5 wt.% H_2O became more forsteritic (from Fo_{89} to Fo_{92}) as the temperature rose from 1400°C to 1570°C at 6.3 GPa; at 7.5 GPa it changed from Fo_{92} to Fo_{95} (Table 3; Fig. 4a). In the greatest part of the samples with 5 wt.% H_2O, the melt-olivine partition coefficient K_D (Fe/Mg) systematically increased with temperature, while the Fe number in olivine became lower (Fig. 4 b). This behavior agrees with trends observed previously in peridotite-CO_2 and peridotite-CO_2-H_2O systems (Brey et al. 2008; Foley et al. 2009; Stagno and Frost 2010). However, K_D deviated notably from those trends toward lower values for the same Fe# of olivine in two water-rich samples. Thus, the FeO content in olivine depended on the temperature and amount of water in the system.

Garnet formed as a subliquidus phase within narrow ranges of temperatures and water contents in some of the experiment runs. It occurred as isometric crystals up to 20 μm in size

299 at temperatures 1400°C and from 100 to 300 μm at 1570°C. The crystals were
300 compositionally uniform and showed no zonation. Small crystals were colorless while large
301 garnets varied in color from pink to mauve. Garnets crystallized in equilibrium with the
302 kimberlite melt had high percentages of pyrope and low percentages of grossular
303 components (Table 3). As the temperature rose, Mg# in garnet also increased systematically
304 (Fig. 4c). The temperature dependence of Mg# in garnet and olivine equilibrated with H_2O-
305 bearing melt agrees well with the calibration model by O'Neill and Wood (1979). The
306 contents of Cr_2O_3 varied from 2.2 to 4.7 wt.% and CaO was from 3.4 to 5.2 wt.% (Table 3).
307 The garnets synthesized in the experiments were compositionally close to mantle garnets
308 transitional between harzburgite and lherzolite suites (Sobolev et al. 1977; Schulze 2003).
309 On the other hand, low concentrations of Cr_2O_3 and high TiO_2 make them similar to garnet
310 megacrysts in kimberlite (Schulze 2003). The microprobe data recalculated following the
311 method from (Finger 1972) show garnet compositions almost free from Fe^{3+}. None of the
312 garnets that formed at pressures 6.3 and 7.5 GPa showed significant Si excess over 3 apfu
313 indicating the absence of solid solutions with majorite.
314 Orthopyroxene was present as a solid phase at all pressures and temperatures in the
315 experiments. Most of the orthopyroxenes were subhedral prismatic colorless crystals, 30-
316 100 μm in lower-temperature runs and up to 300 μm at higher temperatures. It is worth of
317 note that Al_2O_3, Cr_2O_3, MgO, FeO, CaO and Na_2O in the obtained orthopyroxene (Table 3,
318 Fig. 4d, e, f) were very similar to those in its counterpart from mantle xenoliths in kimberlite
319 (Sobolev 1977; Dawson 1980). Al_2O_3 in orthopyroxene increased from 0.4-0.6 to 1.1-1.4
320 wt.% with the temperature rise from 1400°C to 1570-1600°C (Table. 3; Fig. 4f). Note that
321 neither pressure nor water content caused any significant influence on the concentration of

322 Al_2O_3 in kimberlite melt (Fig. 3c). Calcium was constant (from 0.8 to 1.0 wt.%) with
323 temperature rise, while in more hydrous compositions CaO decreased to 0.6 wt.% at
324 relatively low temperatures (Fig. 4e).
325 Note that mass-balance calculations indicated apparently greater Fe loss at higher
326 temperatures and water contents in kimberlite samples (Tables 2, 3). Thus, Fe concentrations
327 in the phases and the Fe and Mg solid-liquid partitioning in samples with Fe loss more than
328 0.01 (Table 2) must be slightly erroneous.
329
330 **DISCUSSION**
331
332 **Magma generation conditions**
333
334 Inasmuch as the used bulk composition of group II kimberlite (Ulmer and Sweeney
335 2002) is basically similar to the potential primary magma (Becker and Le Roex 2006), the
336 reported multiple saturation data may place constraints on the temperatures of magma
337 generation and on the fluid regime in the peridotite source region.
338 The data we obtained indicate that samples at 100°C below the liquidus have "near-
339 liquidus" phase relations (Table 2, Fig. 3). The melting degree of samples at 100°C below
340 the liquidus apparently reached ≥70%. Judging by the revealed trends, the formed melt was
341 compositionally similar to that resulting from complete melting of the samples, as well as to
342 the average composition of close-to-primary magma for group II kimberlite (Becker and Le
343 Roex 2006; Table 1).

Therefore, near-liquidus multiple saturation of group II kimberlite at 6.3 and 7.5 GPa is possible only if it contains no more than 5 wt.% H_2O. The phase composition of group II kimberlite with 5 wt.% H_2O we have observed at 1400-1500°C perfectly agrees with that reported by Ulmer and Sweeney (2002). Note that olivine, garnet, and orthopyroxene crystallized near the liquidus of group II kimberlite are very similar to those in the counterparts from mantle xenoliths in kimberlite. As kimberlite becomes more hydrous, the gap between the liquidus and the appearance of the Ol+Grt+Opx residue in equilibrium with the melt increases from <100°C at 5 wt.% H_2O to ~200°C at 9 wt.% H_2O, both at 6.3 and 7.5 GPa. Garnet is the first phase that becomes unstable at higher water concentrations, while it is its very presence in the source that is required to provide high LREE enrichment of magma (Mitchell 1986; Ringwood et al. 1992). The absence of multiple saturation near the liquidus in the case of more hydrous (>5 wt.% H_2O) compositions with X_{CO2}<0.37 indicates the lack of equilibrium between the magma and garnet harzburgite. Therefore, carbonated garnet harzburgite sources can generate magmas close to the average group II kimberlite only at water contents within 5 wt.%. Note that this result disagrees with the water contents in group II kimberlites from South Africa (7.3 wt.% H_2O at one-sigma error 2.4) reported in (Becker and Le Roex 2006).

Relatively high temperatures of liquidus and multiple saturation of kimberlite suggest that generation of magma with ~5 wt.% H_2O was impossible under an ordinary undisturbed subcontinental thermal regime, at T≤1400°C (Mather et al. 2011). Brey et al. (2009) arrived at a similar conclusion earlier when they studied the influence of water on melting of carbonated peridotite at 6 and 10 GPa. Heat, and possibly also fluid, required to initiate melting and generate kimberlite magmas at 1500-1600°C may have come from

upwelling plumes (Becker and Le Roex 2006; Brey et al. 2009). From the lower liquidus temperatures obtained with group II kimberlite samples containing more than 5 wt.% H_2O, we expect that hydrous multiply saturated kimberlite magma may form already at ~1400-1500°C. For instance, at these temperatures we achieved saturation of the hydrous Udachnaya kimberlite melt with respect to garnet wehrlite residue in 6.3 and 7.5 GPa experiments (Sokol et al. 2013a). Specifically, near-liquidus multiple saturation of this melt was observed at 6.3 GPa when H_2O increased from 6 to 10 wt.% and X_{CO2} decreased from 0.38 to 0.26, while the liquidus became ~200°C lower: 1470°C instead of 1670°C. However, as shown by our experiments, generation of group II kimberlite magma by melting of carbonated harzburgite requires H_2O to be within 5 wt.% (see above).

Generally, our results support the inference of Girnis et al. (1995) that the composition and amount of fluids can strongly affect phase relations near the liquidus of group I kimberlite. Earlier the lack of multiple saturation was noted to be associated with CO_2 increase in the melt. As Girnis et al. (1995) showed, magnesite instead of olivine became stable near the liquidus of group I kimberlite at 5.5 GPa and the molar ratio $CO_2/(CO_2+H_2O)\geq0.7$. In the experiments with low-H_2O samples of the Udachnaya (group I) kimberlite (Sharygin et al. 2013) at 6.5 GPa and $X_{CO2}=0.8$, only Ol+Grt appeared near the liquidus (see above). We have shown, for the first time in this study, that multiple saturation of group II kimberlite magma, with low-degree silica undersaturation, is absent also at high water concentrations and molar ratios $CO_2/(CO_2+H_2O)<0.37$.

There have been different models suggested for specific conditions of kimberlite magma generation. The K-enriched nature of group II kimberlite was attributed to metasomatism by MARID (mica–amphibole–rutile–ilmenite–diopside suite of mantle

390 xenoliths) like melts in earlier publications (Jones et al. 1989; Mitchell 1995; Konzett et al.
391 1998). The model of McCandless (1999), which is based on ages of kimberlite magmatism
392 combined with seismic images and thermal models of subducted slabs, related magma
393 generation with subduction. Judging by their geochemistry, group II kimberlites must be
394 derived from lithospheric mantle source regions metasomatized by melts or fluids associated
395 with ancient subduction events (Becker and Le Roex 2006). The trace-element
396 characteristics of these kimberlites obtained by Coe et al. (2008) imply an affinity to
397 subduction-related calc-alkaline fluids or melts. Tappe et al. (2009) suggested that group II
398 kimberlite magma resulted from melting of metasomatized peridotite that hosted several
399 generations of contrasting vein assemblages (older MARID-type and younger CO_2- and
400 potassic-rich carbonatite vein networks) at the lithospheric base beneath cratons.
401 The formation mechanism of ultrapotassic rocks in the model of Foley (1992) was
402 associated with melting of metasomatic enriched veined lithosphere, the resulting magmas
403 being hybrids of vein and wall-rock components. Ulmer and Sweeney (2002) later explained
404 the carbonate and potassic character of group II kimberlite magma as being produced by a
405 process in which either a carbonate-bearing protolith was invaded by a potassic melt or fluid
406 (probably supercritical), or a potassic protolith (after metasomatism) had been invaded by a
407 carbonatite melt.
408 The generation of highly mobile potassic-rich carbonatite may result from melting of
409 carbonated pelite in the upper part of the slab column (Hammouda and Laporte 2000).
410 Recent experiments (Grassi and Schmidt 2011) have shown that melting of carbonated
411 pelites at depths to 400 km is feasible at extremely hot subduction conditions or when
412 subduction slows down and thermal relaxation sets in. By investigating the solidus of

subducting alkaline carbonatite, Litasov et al. (2013) concluded that their melting may occur in a mantle transition zone. Calcium-rich carbonatite magma can also form on interaction between strongly reduced Fe^0-bearing mantle and subducting carbonate (Palyanov et al. 2013). At adiabatic temperatures, alkali-rich carbonatite will rise into the overlying mantle either by upward percolation (Grassi and Schmidt 2011) or by forming mobile melt diapirs (Litasov et al. 2013).

Oxygen fugacity in the potential source regions of group II kimberlite magma may vary in a broad range. Generally, subcratonic peridotite at the depths of magma generation is strongly reduced, with fO_2 about the Fe-FeO (IW) buffer +1 log unit (Woodland and Koch 2003; McCammon and Kopylova 2004; Yaxley et al. 2012) due to pressure effects on Fe^{2+}–Fe^{3+} equilibria in garnet. It is diamond, rather than carbonate minerals, that is stable in the peridotite mantle at this oxygen fugacity (Luth 2004; Stagno et al. 2013). On the other hand, the redox conditions in the peridotite source regions are subject to local changes as a result of multiple metasomatic events. MARID-type xenolith minerals have high Fe^{3+} enrichment, as Dawson (1980) reported long ago. More recently, MARID assemblages have been inferred to form at oxygen fugacities outside the diamond stability field, and even above the FMQ (fayalite-magnetite-quartz) buffer (Woodland and Koch 2003; Creighton et al. 2009). Infiltration of metasomatic fluids/melts into the subcratonic diamondiferous lithospheric mantle can convert reduced anhydrous harzburgite into variably oxidized phlogopite-bearing lherzolite, which was predicted, for example, for the Kaapvaal craton (Creighton et al. 2009). Carbonatite melts, rich in incompatible elements, potassium, and calcium, can percolate into the peridotite source region and cause its oxidation (Frost and McCammon

2008; Rohrbach and Schmidt 2011) and increase the clinopyroxene/orthopyroxene ratio (Thibault et al. 1992).

Magma generated as a result of redox reactions must be rich in volatiles and supersaturated with respect to carbon, which is an effective environment for diamond and graphite formation (Pal'yanov et al. 1999; Palyanov et al. 2007; Sokol and Palyanov 2008; Palyanov and Sokol 2009). Note that some of group II kimberlites are actually diamond-bearing. Therefore, the final stage of the formation and separation of carbonated magma should proceed at fO_2 about the EMOD buffer (Stagno et al. 2013), this being exactly the oxygen fugacity we have reproduced in our multiple saturation experiments with group II kimberlite.

Water sources

The interaction of the percolating carbonatite with the potential peridotite source of group II kimberlite can produce water. Water may reside in pre-existing hydrous minerals formed by metasomatism during reaction with MARID-like melts (Mitchell 1995). Phlogopite is stable in the presence of carbonate melt in the peridotite source at the 180–200 km depths under subcontinental thermal conditions (Grassi and Schmidt 2011). However, supersolidus temperatures may initiate a peritectic reaction (Ulmer and Sweeney 2002)

$$2\ \text{phlogopite} + MgCO_2 \rightarrow 2\ \text{opx} + \text{olivine} + \text{garnet} + K_2CO_3\ (L) + 2\ H_2O\ (L), \quad (1)$$

which provides water extraction from a phlogopite-bearing source region. As Ulmer and Sweeney (2002) noted, the absence of phlogopite (or K-richterite) in equilibrium with a garnet harzburgite residue close to the liquidus is not a proof of its absence in the mantle

458 protolith. This mechanism, however, is poorly applicable to magmas rich in H_2O. Melting of
459 carbonated phlogopite lherzolite in experiments reported by (Thibault et al. 1992) yielded 4
460 wt.% of alkaline dolomitic melt at 3.0 GPa and 1100°C, with only ~2.7 wt.% H_2O, which is
461 much lower than the estimates for the primary magma of group II kimberlite from (Becker
462 and Le Roex 2006).

463 Nominally anhydrous minerals (NAMs) of the mantle protolith, which contain water as
464 hydrated defects (Hirschmann et al. 2005; 2009; Green et al. 2010; Peslier et al. 2010; Ardia
465 et al. 2012), are a potential additional water source. Extraction from NAMs becomes
466 possible if they have very low water partition coefficient between NAMs and carbonatite
467 melt (Sokol et al. 2013b). The efficiency of this mechanism depends on H_2O concentration
468 in the protolith and on $CO_2/(CO_2+SiO_2)$ molar ratios in the melt. The capacity of this water
469 source can be evaluated taking into account that the potential peridotite source region
470 beneath the Kaapvaal craton stores 80-100 ppm of water (Peslier et al. 2010) and that group
471 II kimberlites, in turn, are relatively depleted in CO_2 and enriched in SiO_2. The
472 experimentally determined partition coefficient between olivine and harzburgite saturated
473 kimberlite melt ($D^{ol/melt}_{H2O}$) is ~0.003 (Sokol et al. 2013b). If we assume, in the first
474 approximation, that $D^{per/melt}_{H2O} \approx D^{ol/melt}_{H2O}$ (for olivine-rich peridotite), generation of magma
475 with 5-7 wt.% H_2O would require either greater water contents in the source region or
476 somewhat lower $D^{per/melt}_{H2O}$ partitioning. The latter would be possible with a primary magma
477 slightly more carbonated than it is commonly presumed (Becker and Le Roex 2006), given
478 that $D^{ol/melt}_{H2O}$ depends on the $CO_2/(CO_2+SiO_2)$ molar ratios in the melt (Sokol et al. 2013b).

479 Acting jointly, these factors could maintain generation of a hydrous kimberlite magma.
480 Furthermore, the equilibrium in reaction (1) may shift left as the water concentration in the

481 K-rich carbonate-silicate melt rises above some critical level. As a result, new portions of
482 hydrous phases (phlogopite and/or K-richterite) may form in the source mantle and provide
483 buffering of K and H_2O contents in the magma.

484

485 **IMPLICATIONS**
486

487 Kimberlite genesis attracts attention of geoscientists as its mechanisms have
488 implications for the global evolution of subcratonic lithosphere and asthenosphere. It is
489 especially important in this respect to constrain the potential temperature and fluid
490 conditions of kimberlite magma generation. The relatively high temperatures of liquidus and
491 multiple saturation of group II kimberlite we have revealed suggest that generation of group
492 II kimberlite magma may occur by partial melting of carbonated (metasomatized) garnet
493 harzburgite at pressures from 6.3 to 7.5 GPa, temperatures about 1500-1600°C, and no more
494 than 5 wt.% H_2O in the melt. The absence of multiple saturation near the liquidus in the case
495 of more hydrous (>5 wt.% H_2O) compositions with X_{CO2}<0.37 indicates the lack of
496 equilibrium between the magma and garnet harzburgite. Thus, the ordinary undisturbed
497 subcontinental thermal regime cannot have maintained generation of group II kimberlite
498 magma. The heat (and fluids) required to initiate melting and generate kimberlite magmas
499 may have come from upwelling plumes (Becker and Le Roex 2006; Brey et al. 2009).
500 Interaction of K-Ca-rich carbonatite melt, infiltrating from a deeper mantle source, with a
501 peridotite protolith containing H_2O in nominally anhydrous minerals and, possibly, also in
502 phlogopite, produced water in the necessary amounts.

503

504 **ACKNOWLEDGEMENTS**

505 The authors thank Yury Borzdov and Alexander Khokhryakov for their assistance
506 throughout the study. We are indebted to Elena Nigmatulina (IGM SB RAS) for assistance
507 with microprobe analysis. We thank Greg Yaxley and Gerhard Brey for their in-depth
508 reviews and helpful comments. This research was supported by grants of the Siberian
509 Branch of the Russian Academy of Sciences (No. 31 and 67.3.1).
510

REFERENCES

Ardia, P., Hirschmann, M.M., Withers, A.C. and Tenner, T.J. (2012) H_2O storage capacity of olivine at 5-8 GPa and consequences for dehydration partial melting of the upper mantle. Earth and Planetary Science Letters, 345, 104-116.

Becker, M. and Le Roex, A.P. (2006) Geochemistry of South African on- and off-craton, Group I and Group II kimberlites: Petrogenesis and source region evolution. Journal of Petrology, 47, 673-703.

Brey, G.P., Bulatov, V.K., Girnis, A.V. and Lahaye, Y. (2008) Experimental melting of carbonated peridotite at 610 GPa. Journal of Petrology, 49, 797-821.

Brey, G.P., Bulatov, V.K. and Girnis, A.V. (2009) Influence of water and fluorine on melting of carbonated peridotite at 6 and 10 GPa. Lithos, 112, 249-259.

Brey, G.P., Bulatov, V.K. and Girnis, A.V. (2011) Melting of K-rich carbonated peridotite at 6-10 GPa and the stability of K-phases in the upper mantle. Chemical Geology, 281, 333-342.

Canil, D. and Scarfe, C.M. (1990) Phase-relations in peridotite + CO_2 systems to 12 GPa - implications for the origin of kimberlite and carbonate stability in the earths upper mantle. Journal of Geophysical Research-Solid Earth and Planets, 95(B10), 15805-15816.

Coe, N., Le Roex, A., Gurney, J., Pearson, D.G. and Nowell, G. (2008) Petrogenesis of the Swartruggens and Star Group II kimberlite dyke swarms, South Africa: constraints from whole rock geochemistry. Contributions to Mineralogy and Petrology, 156, 627-652.

534 Creighton, S., Stachel, T., Matveev, S., Hofer, H., McCammon, C. and Luth, R.W. (2009)
535 Oxidation of the Kaapvaal lithospheric mantle driven by metasomatism.
536 Contributions to Mineralogy and Petrology, 157, 491-504.
537 Dawson, J.B. (1980) Kimberlites and their xenoliths, 252 p. Springer, Berlin,
538 Eggler, D.H. and Wendlandt, R.F. (1979) Experimental studies on the relationships between
539 kimberlite magma and partial melting of peridotite. In F.R. Boyd and H.O.A. Meyer,
540 Eds., Kimberlites, Diatremes and Diamonds: Their Geology, Petrology, and
541 Geochemistry 1, p. 331–378. American Geophysical Union, Washington.
542 Finger, L.W. (1972) The uncertainty in the calculated ferric iron content of a microprobe
543 analysis, p. 600–603.Carnegie Institution of Washington Year Book 1971.
544 Foley, S. (1992) Vein-plus-wall-rock melting mechanisms in the lithosphere and the origin
545 of potassic alkaline magmas. Lithos, 28, 435-453.
546 Foley, S.F., Yaxley, G.M., Rosenthal, A., Buhre, S., Kiseeva, E.S., Rapp, R.P. and Jacob,
547 D.E. (2009) The composition of near-solidus melts of peridotite in the presence of
548 CO_2 and H_2O between 40 and 60 kbar. Lithos, 112, 274-283.
549 Frost, D.J. and McCammon, C.A. (2008) The redox state of Earth's mantle. Annual Review
550 of Earth and Planetary Sciences, 36, 389-420.
551 Funk, S.P. and Luth, R.W. (2012) An experimental study of a minette from the Milk River
552 area, southern Alberta, Canada. Contributions to Mineralogy and Petrology, 164
553 999-1009.
554 Girnis, A.V., Brey, G.P. and Ryabchikov, I.D. (1995) Origin of Group 1A kimberlites:
555 Fluid-saturated melting experiments at 45-55 kbar. Earth and Planetary Science
556 Letters, 134, 283-296.

557 Girnis, A.V., Bulatov, V.K. and Brey, G.P. (2011) Formation of primary kimberlite melts -
558 Constraints from experiments at 6-12 GPa and variable CO_2/H_2O. Lithos, 127, 401-
559 413.
560 Grassi, D. and Schmidt, M.W. (2011) The Melting of Carbonated Pelites from 70 to 700 km
561 Depth. Journal of Petrology, 52, 765-789.
562 Green, D.H., Hibberson, W.O., Kovacs, I. and Rosenthal, A. (2010) Water and its influence
563 on the lithosphere-asthenosphere boundary. Nature, 467, 448-451.
564 Gudfinnsson, G.H. and Presnall, D.C. (2000) Melting behaviour of model lherzolite in the
565 system $CaO-MgO-Al_2O_3-SiO_2-FeO$ at 0.7-2.8 GPa. Journal of Petrology, 41, 1241-
566 1269.
567 Hammouda, T. and Laporte, D. (2000) Ultrafast mantle impregnation by carbonatite melts.
568 Geology, 28, 283-285.
569 Hirschmann, M.M., Aubaud, C. and Withers, A.C. (2005) Storage capacity of H_2O in
570 nominally anhydrous minerals in the upper mantle. Earth and Planetary Science
571 Letters, 236, 167-181.
572 Hirschmann, M.M., Tenner, T., Aubaud, C. and Withers, A.C. (2009) Dehydration melting
573 of nominally anhydrous mantle: The primacy of partitioning. Physics of the Earth
574 and Planetary Interiors, 176, 54-68.
575 Jones, A.P. (1989) Upper mantle enrichment by kimberlitic or carbonatitic magmatism. In
576 K. Bell, Ed., Carbonatites: Genesis and evolution, p. 448–463. Unwin Hyman.
577 Kamenetsky, V.S., Kamenetsky, M.B., Weiss, Y., Navon, O., Nielsen, T.F.D. and Mernagh,
578 T.P. (2009) How unique is the Udachnaya-East kimberlite? Comparison with

kimberlites from the Slave Craton (Canada) and SW Greenland. Lithos, 112, 334-346.

Kennedy, C.S. and Kennedy, G. (1976) The equilibrium boundary between graphite and diamond. Journal of Geophysical Research, 81, 2467–2470

Litasov, K.D., Shatskiy, A., Ohtani, E. and Yaxley, G.M. (2013) The Solidus of Alkaline Carbonatite in the Deep Mantle. Geology, 41, 79-82.

Luth, RW. (2004) Mantle volatiles – distribution and consequences. In H.D. Holland and K.K. Turekian, Eds., Treatise on Geochemistry, vol. 2, p. 319–361. Elsevier.

Mather, K.A., Pearson, D.G., McKenzie, D., Kjarsgaard, B.A. and Priestley, K. (2011) Constraints on the depth and thermal history of cratonic lithosphere from peridotite xenoliths, xenocrysts and seismology. Lithos, 125, 729-742.

McCammon, C. and Kopylova, M.G. (2004) A redox profile of the Slave mantle and oxygen fugacity control in the cratonic mantle. Contributions to Mineralogy and Petrology, 148, 55-68.

McCandless, T.E. (1999) Kimberlites: mantle expressions of deepseated subduction. In J.J. Gurney, J.L. Gurney, M.D. Pascoe and S.H. Richardson, Eds., Proceedings of the 7th international kimberlite conference, vol 2., p. 545–549. Red Roof Publishers, Cape Town.

Mitchell, R.H. (1986) Kimberlites: mineralogy, geochemistry and petrology, 441 p. Plenum Press, New York.

Mitchell, R.H. (1995) Kimberlites, orangeites, and related rocks, 410 p. Plenum Press.

O'Neill, H.C. and Wood, B.J. (1979) An experimental study of Fe-Mg partitioning between garnet and olivine and its calibration as a geothermometer. Contributions to Mineralogy and Petrology, 70, 59–70.

Pal'yanov, Y.N., Sokol, A.G., Borzdov, Y.M., Khokhryakov, A.F. and Sobolev, N.V. (1999) Diamond formation from mantle carbonate fluids. Nature, 400, 417-418.

Palyanov, Y.N., Shatsky, V.S., Sobolev, N.V. and Sokol, A.G. (2007) The role of mantle ultrapotassic fluids in diamond formation. Proceedings of the National Academy of Sciences of the United States of America, 104, 9122-9127.

Palyanov, Y.N. and Sokol, A.G. (2009) The effect of composition of mantle fluids/melts on diamond formation processes. Lithos, 112, 690-700.

Palyanov, Y.N., Borzdov, Y.M., Khokhryakov, A.F., Kupriyanov, I.N. and Sokol, A.G. (2010) Effect of Nitrogen Impurity on Diamond Crystal Growth Processes. Crystal Growth & Design, 10, 3169-3175.

Palyanov, Y.N., Bataleva, Y.V., Sokol, A.G., Borzdov, Y.M., Kupriyanov, I.N., Reutsky, V.N. and Sobolev, N.V. (2013) Mantle-slab interaction and redox mechanism of diamond formation. Proceedings of the National Academy of Sciences of the United States of America, 110, 20408-20413.

Peslier, A.H., Woodland, A.B., Bell, D.R. and Lazarov, M. (2010) Olivine water contents in the continental lithosphere and the longevity of cratons. Nature, 467, 78-U108.

Ringwood, A.E., Kesson, S.E., Hibberson, W. and Ware, N. (1992) Origin of kimberlites and related magmas. Earth and Planetary Science Letters, 113, 521-538.

Rohrbach, A. and Schmidt, M.W. (2011) Redox freezing and melting in the Earth's deep mantle resulting from carbon-iron redox coupling. Nature, 472, 209-212.

623 Schulze, D.J. (2003) A classification scheme for mantle-derived garnets in kimberlite: a tool
624 for investigating the mantle and exploring for diamonds. Lithos, 71, 195-213.
625 Sharygin, I.S., Litasov, K.D., Shatskiy, A.F., Golovin, A.V., Ohtani, E. and Pokhilenko,
626 N.P. (2013) Melting of kimberlite of the Udachnaya-East pipe: Experimental study at
627 3-6.5 GPa and 900-1500 degrees C. Doklady Earth Sciences, 448, 200-205.
628 Smith, C.B., Gurney, J.J., Barton, E.S. and Bristow, J.W. (1985) Geochemical character of
629 southern African kimberlites: A new approach based on isotopic constraints. Trans.
630 Geol. Soc. South Africa, 88, 267–280.
631 Sobolev, N.V. (1977) The Deep-Seated Inclusions in Kimberlites and the Problem of the
632 Composition of the Upper Mantle, 304 p. American Geophysics Union, Washington.
633 Sokol, A.G., Palyanov, Y.N. and Surovtsev, N.V. (2007) Incongruent melting of gallium
634 nitride at 7.5 GPa. Diamond and Related Materials, 16, 431-434.
635 Sokol, A.G. and Pal'yanov, Yu.N. (2008) Diamond formation in the system MgO–SiO_2–
636 H_2O–C at 7.5 GPa and 1600°C. Contribution to Mineralogy and Petrology, 155, 33–
637 43.
638 Sokol, A.G., Kupriyanov, I.N., Palyanov, Y.N., Kruk, A.N. and Sobolev, N.V. (2013a)
639 Melting experiments on the Udachnaya kimberlite at 6.3-7.5 GPa: implications for
640 the role of H_2O in magma generation and formation of hydrous olivine. Geochimica
641 Et Cosmochimica Acta, 101, 133-155.
642 Sokol A.G., Kupriyanov, I.N. and Palyanov, Yu.N. (2013b) Partitioning of H2O between
643 olivine and carbonate–silicate melts at 6.3 GPa and 1400°C: Implications for
644 kimberlite formation. Earth and Planetary Science Letters, 383, 58–67.

645 Stagno, V. and Frost, D.J. (2010) Carbon speciation in the asthenosphere: Experimental
646 measurements of the redox conditions at which carbonate-bearing melts coexist with
647 graphite or diamond in peridotite assemblages. Earth and Planetary Science Letters,
648 300, 72-84.
649 Stagno, V., Ojwang, D.O., McCammon, C.A. and Frost, D.J. (2013) The oxidation state of
650 the mantle and the extraction of carbon from Earth's interior. Nature, 493, 84-88.
651 Tappe, S., Steenfelt, A., Heaman, L.M. and Simonetti, A. (2009) The newly discovered
652 Jurassic Tikiusaaq carbonatite-aillikite occurrence, West Greenland, and some
653 remarks on carbonatite-kimberlite relationships. Lithos, 112, 385-399.
654 Thibault, Y., Edgar, A.D. and Lloyd, F.E. (1992) Experimental investigation of melts from a
655 carbonated phlogopite lherzolite - implications for metasomatism in the continental
656 lithospheric mantle. American Mineralogist, 77, 784-794.
657 Ulmer, P. and Sweeney, R.J. (2002) Generation and differentiation of group II kimberlites:
658 Constraints from a high-pressure experimental study to 10 GPa. Geochimica Et
659 Cosmochimica Acta, 66, 2139-2153.
660 Woodland, A.B. and Koch, M. (2003) Variation in oxygen fugacity with depth in the upper
661 mantle beneath the Kaapvaal craton, Southern Africa. Earth and Planetary Science
662 Letters, 214, 295-310.
663 Yaxley, G.M., Berry, A.J., Kamenetsky, V.S., Woodland, A.B. and Golovin, A.V. (2012)
664 An oxygen fugacity profile through the Siberian Craton - Fe K-edge XANES
665 determinations of $Fe^{3+}/\Sigma Fe$ in garnets in peridotite xenoliths from the Udachnaya
666 East kimberlite. Lithos, 140, 142-151.
667
668

669 **FIGURE CAPTIONS**

670 Fig. 1. Scanning electron micrographs of the recovered samples. a: run # 1350 (6.3 GPa,
671 1570°C, 5 wt.% H_2O); b : run # 1341 (6.3 GPa, 1470°C, 5 wt.% H_2O); c: run # 1497-1 (6.3
672 GPa, 1450°C, 7 wt.% H_2O); d: run # 1619-1 (6.3 GPa, 1570°C, 7 wt.% H_2O); e: run # 1621-
673 1 (7.5 GPa, 1570°C, 5 wt.% H_2O); f: run # 1495-2 (7.5 GPa, 1400°C, 9 wt.% H_2O).
674 Abbreviations stand for: Ol = olivine; Cpx = clinopyroxene; Grt = garnet; Pv = perovskite;
675 Liq = quenched liquid.

676 Fig. 2. Experimentally determined phase relations in group II kimberlite at 6.3 GPa (a)
677 and 7.5 GPa (b), at different H_2O contents. Dashed lines show phase boundaries (the first
678 occurrence of the phase labeled on the curve). Bold dashed lines indicate positions of
679 liquidi. Squares correspond to assemblages present in various regions of the phase diagram;
680 solid sectors = phase present; void sectors = phases absent from paragenesis. Ol = olivine;
681 Opx = orthopyroxene; Grt = garnet; L = quenched liquid.

682 Fig. 3. Liquid compositions as a function of experimental temperature (the analyses were
683 not normalized to 100 wt.% volatile-free compositions). a: SiO_2 and MgO concentrations in
684 the melt at 6.3 GPa; b: SiO_2 and MgO in the melt at 7.5 GPa; c: CaO and Al_2O_3
685 concentrations in the melt at 6.3 GPa; d: CaO and Al_2O_3 in the melt at 7.5 GPa; e: Ca# of the
686 melt at 6.3 and 7.5 GPa; f: Al/(Al+Si+Mg+Fe+Ca) vs. (Mg+Fe+Ca)/(Si+Mg+Fe+Ca) (at.)
687 diagram of the melt at 6.3 and 7.5 GPa; g: Mg# of the melt at 6.3 GPa; h: Mg# of the melt at
688 7.5 GPa. Data for 6.3 GPa and 1400°C are from (Sokol et al., 2013b). Numbers shown near
689 the symbols represent water concentration (wt.%) in the starting kimberlite. The symbol
690 sizes are proportional to H_2O concentrations. Dash lines connect data points for kimberlite

691 with 5 wt.% H_2O. G-D are compositions for runs # 1350 and # 1621-1, where graphite-to-
692 diamond conversion in graphite liners was observed.

693 Fig. 4. Compositions of olivine, garnet and orthopyroxene. a: Mg# of olivine as a
694 function of temperature (Mg# is molar MgO/(MgO+FeO)); b: Fe–Mg partition coefficient
695 ($K_D=(X_{Fe(melt)}\cdot X_{Mg(olivine)})/(X_{Fe(olivine)}\cdot X_{Mg(melt)})$ between melt and olivine as a function of Fe#
696 of olivine (Fe# is molar FeO/(MgO+FeO)); c: Mg# of garnet as a function of temperature
697 (Mg# is molar MgO/(MgO+FeO+CaO)); d: Mg# of orthopyroxene as a function of
698 temperature; e: CaO concentrations in orthopyroxene as a function of temperature; f: Al_2O_3
699 concentrations in orthopyroxene as a function of temperature. Data for 6.3 GPa and 1400°C
700 are from (Sokol et al., 2013b). Numbers shown near the symbols represent water
701 concentration (wt.%) in the starting kimberlite. The symbol sizes are proportional to H_2O
702 concentrations. Dashed lines connect data points for kimberlite with 5 wt.% H_2O. G-D are
703 compositions for runs # 1350 and # 1621-1, where graphite-to-diamond conversion in
704 graphite liners was observed.

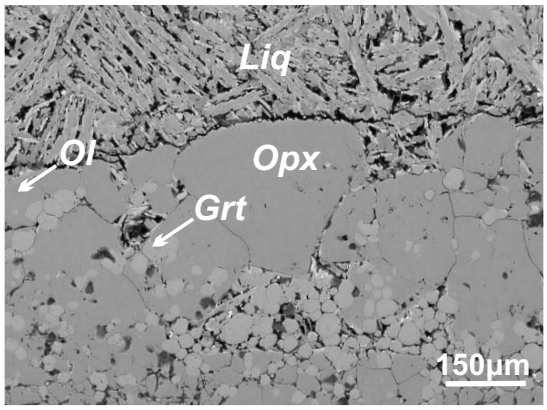
Liq
Ol
Opx
Grt
150µm

a

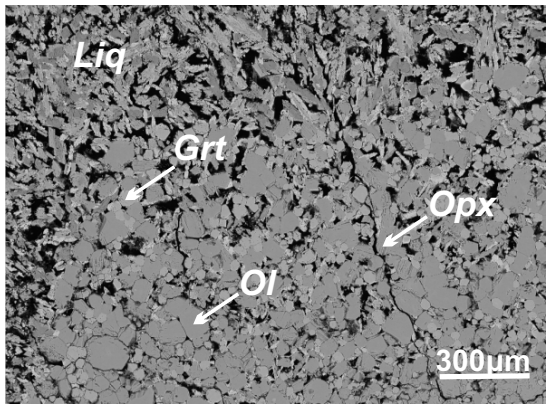
Liq
Grt
Opx
Ol
300µm

b

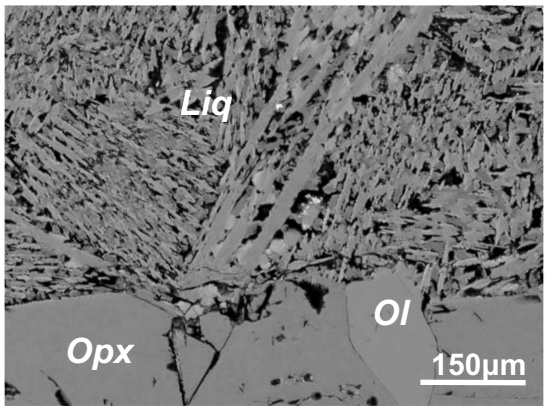
Liq
Ol
Opx
150µm

c

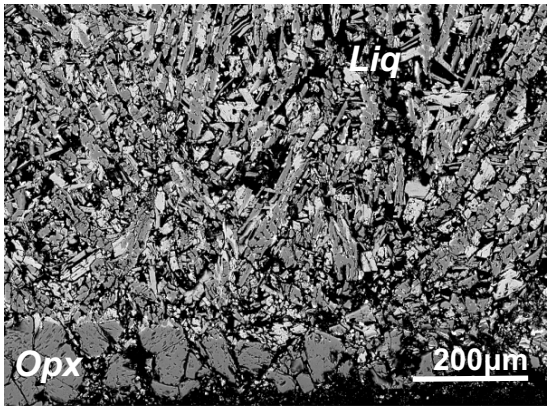
Liq
Opx
200µm

d

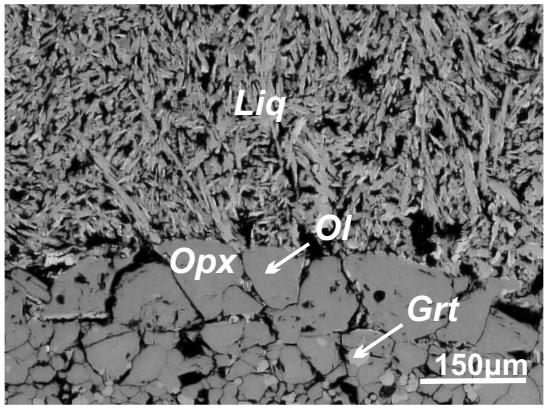
Liq
Ol
Opx
Grt
150µm

e

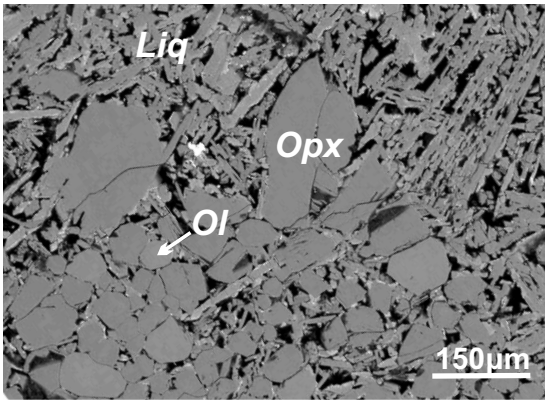
Liq
Opx
Ol
150µm

f

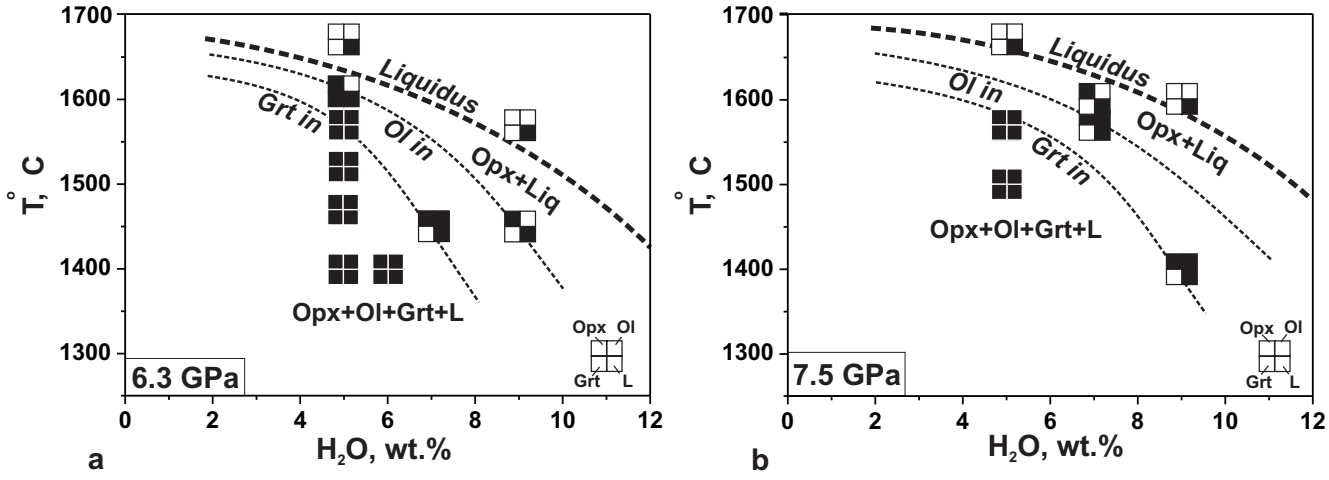
1700
1600
1500
1400
1300
T, °C
Liquidus
Grt in
Ol in
Opx+Liq
Opx+Ol+Grt+L
6.3 GPa
Opx Ol
Grt L
0
2
4
6
8
10
12
H2O, wt.%
a
7.5 GPa
b

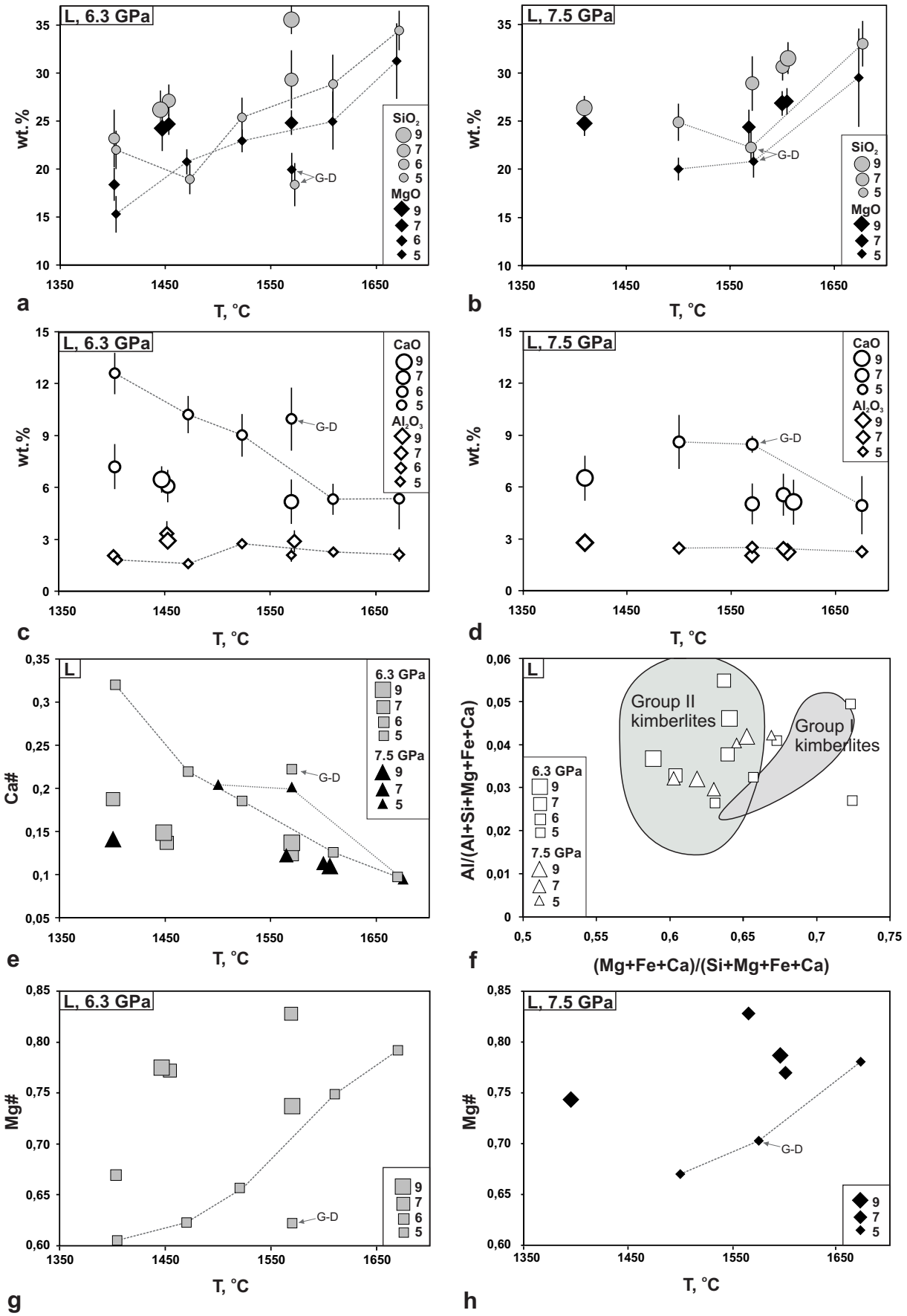
L, 6.3 GPa
L, 7.5 GPa
wt.%
T, °C
SiO2
MgO
CaO
Al2O3
G-D
a
b
c
d
L
6.3 GPa
7.5 GPa
Ca#
e
Group II kimberlites
Group I kimberlites
Al/(Al+Si+Mg+Fe+Ca)
(Mg+Fe+Ca)/(Si+Mg+Fe+Ca)
f
Mg#
g
h

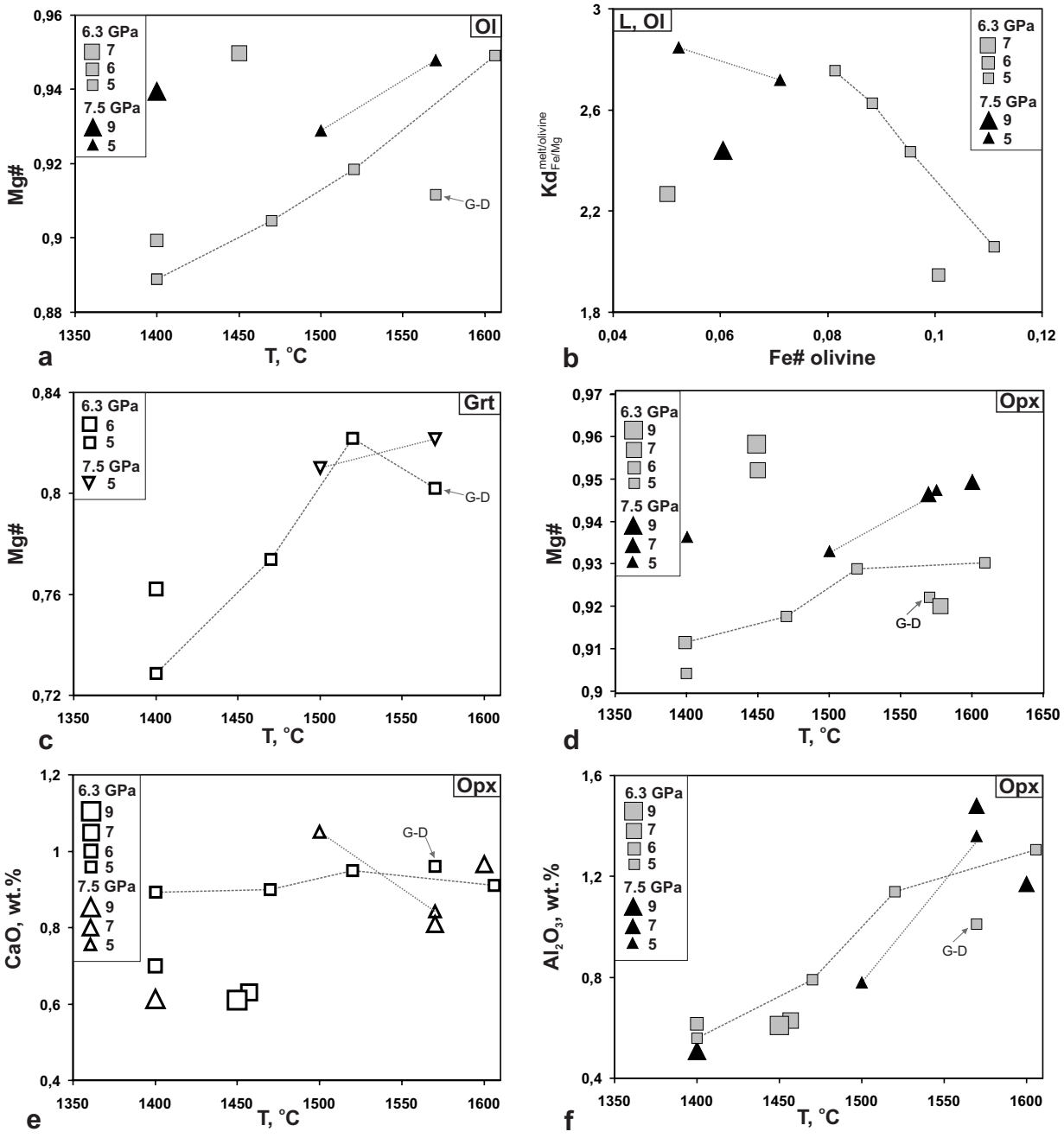
Ol
6.3 GPa
7
6
5
7.5 GPa
9
5
G-D
Mg#
T, °C
a
L, Ol
Kd melt/olivine Fe/Mg
Fe# olivine
b
Grt
c
Opx
d
CaO, wt.%
e
Al2O3, wt.%
f

Table 1. Bulk compositions of group II kimberlite from South Africa and initial compositions for multiple saturation experiments.

	Smith et al., (1985), average	Becker and Le Roex (2006)			A	B_1	B_2	B_3	B_4
		average on-craton	close-to-primary magma	1 SD					
SiO_2	36.30	35.32	33.89	4.80	35.48	35.48	35.09	34.71	33.97
TiO_2	1.00	1.23	1.77	1.50	1.00	1.00	0.99	0.98	0.96
Cr_2O_3	-	0.25	0.23	0.09	0.30	0.30	0.30	0.29	0.29
Al_2O_3	3.20	2.71	3.76	2.00	3.16	3.16	3.13	3.09	3.03
FeO	7.60	7.96[a]	8.76 [a]	0.60	8.22	8.22	8.13	8.04	7.87
MnO	0.20	0.16	0.18	0.05	0.24	0.24	0.24	0.23	0.23
MgO	29.70	29.00	23.15	4.20	29.10	29.10	28.78	28.47	27.86
NiO	-	0.18	0.14	0.06	0.44	0.44	0.44	0.43	0.42
CaO	6.00	6.98	9.96	2.00	5.88	5.88	5.81	5.75	5.63
Na_2O	0.10	0.29	0.25	0.24	0.93	0.93	0.92	0.91	0.89
K_2O	3.20	2.61	3.63	1.40	3.17	3.17	3.13	3.10	3.03
P_2O_5	1.10	1.22	1.85	0.80	-	-	-	-	-
CO_2	3.60	4.65	4.21	2.80	7.13	7.13	7.05	6.98	6.83
H_2O	6.80	6.02	7.33	2.40	4.97	4.97	6.00	7.01	9.01
Total	98.80	90.63	90.35		100.02	100.02	100.00	100.00	100.00
Mg #	0.87	0.78	0.85		0.86	0.86	0.86	0.86	0.86
CS	0.10	0.136	0.12		0.20	0.20	0.20	0.20	0.20
X_{CO2}	0.18	0.23	0.19		0.37	0.37	0.32	0.29	0.24

Notes: A - initial compositions for multiple saturation experiments used by Ulmer and Sweeney (2002); B_1-B_4 - initial compositions used in this study.
Mg# is molar MgO /(MgO+FeO) ratio; CS is CO_2/SiO_2 wt.%; X_{CO2} is molar ration of $CO_2/(CO_2+H_2O)$;
1 SD - associated one standard deviations of close-to-primary magma.
[a] given as Fe_2O_3.

Table 2. Conditions of experiments and phase compositions of run products.

Run	Conditions				Weight fractions of phase				Fe loss[a]
	P (GPa)	T (°C)	Duration (h)	H_2O (wt.%)	Ol	Opx	Grt	Liq	
1341	6.3	1470	40	5	0.22	0.25	0.1	0.43	<0.01
1343	6.3	1520	40	5	0.17	0.2	0.06	0.57	<0.01
1350	6.3	1570	40	5	0.21	0.25	0.1	0.44[b]	<0.01
1667	6.3	1610	1.5	5	0.05	0.15	-	0.80	<0.01
1500	6.3	1670	1	5	-	-	-	1	<0.01
1497-1	6.3	1450	40	7	0.05	0.2	-	0.75	0.03
1619-1	6.3	1570	2	7	-	0.19	-	0.81	0.02
1497-2	6.3	1450	40	9	-	0.23	-	0.77	0.03
1619-2	6.3	1570	2	9	-	-	-	1	<0.01
1489	7.5	1500	40	5	0.16	0.23	0.03	0.58	0.01
1621-1	7.5	1570	40	5	0.09	0.23	0.01	0.67 [b]	0.02
1501	7.5	1670	1	5	-	-	-	1	<0.01
1621-2	7.5	1570	40	7	0.07	0.18	-	0.75	0.04
1625-1	7.5	1600	2	7	-	0.17	-	0.83	0.01
1495-2	7.5	1400	40	9	0.05	0.25	-	0.7	0.02
1625-2	7.5	1600	2	9	-	-	-	1	<0.01

Notes: Phases: Liq – melt; Ol – olivine; Opx – ortopyroxene; Grt – garnet;
[a] - weight fractions of Fe^0 loss from the system due to alloying with Pt capsule;
[b] - graphite-to-diamond conversion in graphite containers.

Table 3. Average compositions (wt.%) of olivine (Ol), garnet (Grt), ortopyroxene (Opx) and liquid (Liq) from melting experiments of this study.

Run	Phase (n)	SiO_2	TiO_2	Cr_2O_3	Al_2O_3	FeO	MnO	MgO	CaO	Na_2O	K_2O	Total	Mg#	Ca#
1341	Ol(22)	40.3 (3)	0.02 (1)	0.04 (2)	-	9.2 (2)	0.12 (2)	48.9 (4)	0.1 (5)	-	-	98.72	0.90	-
1341	Opx(14)	57.3 (2)	0.07 (5)	0.16 (7)	0.79 (3)	5.5 (2)	0.14 (3)	34.5 (4)	0.9 (3)	0.18 (4)	-	99.61	0.92	-
1341	Grt(14)	42.7 (2)	0.53 (1)	2.24 (5)	20.5 (1)	6.8 (3)	0.30 (4)	22.6 (4)	3.9 (1)	0.08 (4)	-	99.66	0.77	0.10
1341	Liq(8)	19 (1)	1.9 (4)	0.09 (1)	1.6 (3)	9.5 (8)	0.23 (1)	21 (1)	10 (1)	1.3[a]	4.1[a]	68.63	0.80	0.22
1343	Ol(9)	41.0 (2)	0.02 (1)	0.05 (2)	-	8.0 (1)	0.12 (1)	50.5 (4)	0.11 (1)	-	-	99.69	0.92	-
1343	Opx(10)	57.7 (3)	0.06 (1)	0.22 (3)	1.1 (1)	4.8 (3)	0.13 (1)	35.0 (4)	0.9 (5)	0.19 (4)	-	100.13	0.93	-
1343	Grt(6)	43.5 (2)	0.37 (3)	2.39 (8)	21.1 (2)	5. 6 (1)	0.24 (2)	24.3 (2)	3.0 (2)	0.07 (3)	-	100.54	0.82	0.07
1343	Liq(5)	25 (2)	1.5 (4)	0.13□ (2)	2.8 (3)	10.0 (7)	0.27 (3)	23 (1)	9 (1)	0.9[a]	3.3[a]	76.23	0.80	0.19
1350	Ol(10)	41.1 (1)	0.01 (1)	0.04 (1)	-	8.6 (1)	0.13 (1)	49.9 (3)	0.10 (1)	-	-	99.8	0.91	-
1350	Opx(11)	57.2 (7)	0.08 (3)	0.19 (3)	1.0 (1)	5.2 (4)	0.14 (3)	34.7 (3)	0.96 (1)	0.17 (2)	-	100.19	0.92	-
1350	Grt(13)	43.5 (3)	0.48 (4)	2.22 (1)	20.6 (1)	6.1 (2)	0.27 (3)	23.8 (4)	3.4 (2)	-	-	100.5	0.80	0.08
1350	Liq(6)	18 (2)	2.1 (4)	0.08 (2)	2.9 (6)	9.0 (9)	0.25 (4)	20 (2)	10 (2)	1.5[b]	5.0[b]	69.08	0.80	0.22
1667	Ol(7)	41.4(3)	0.01(1)	0.08(1)	-	5.3(3)	0.10(2)	51.7(5)	0.07(3)	-	-	98.66	0.95	-
1667	Opx(5)	57.6(6)	0.06(2)	0.22(2)	1.3(2)	4.7(3)	0.13(2)	34.6(4)	0.9(1)	0.21(2)	-	99.72	0.93	0.12
1667	Liq(6)	29(3)	0.9(2)	0.24(4)	2.3(3)	7.8(4)	0.27(4)	25.(3)	5(2)	1.3[a]	3.74[a]	75.51	0.85	0.12
1500	Liq(7)	34 (2)	0.9 (3)	0.30 (5)	2.1 (4)	7.9 (4)	0.24 (3)	31 (4)	5 (2)	0.9[a]	3.2[a]	86.61	0.79	0.10
1497-1	Ol(6)	41.7 (1)	0.03 (1)	0.11 (3)	-	4.9 (1)	0.16 (3)	52.5 (2)	0.10 (1)	-	-	99.67	0.95	-
1497-1	Opx(5)	58.9 (2)	0.06 (1)	0.22 (1)	0.63 (2)	3.3 (1)	0.14 (1)	36.4 (1)	0.7 (2)	0.13 (1)	0.09 (5)	100.48	0.95	-
1497-1	Liq(7)	27 (2)	1.1 (1)	0.28 (3)	3.6 (4)	5.3 (3)	0.20 (3)	25 (1)	6.1 (9)	1.2[a]	3.8[a]	73.41	0.89	0.14
1619-1	Opx(5)	57.7 (4)	0.07 (1)	0.8 (1)	0.8 (2)	4.4 (2)	0.17 (1)	35.0 (2)	0.90 (3)	0.17 (1)	-	100.03	0.92	-
1619-1	Liq(7)	29 (3)	0.7 (1)	0.24 (4)	2.1 (3)	2.6 (1)	0.19 (2)	25 (1)	5 (1)	0.9[a]	3.4[a]	69.54	0.94	0.12
1497-2	Opx(7)	58.4 (4)	0.06 (1)	0.23 (4)	0.6 (2)	2.9 (2)	0.15 (2)	36.8 (3)	0.60 (2)	0.15 (6)	-	99.96	0.96	-
1497-2	Liq(6)	26.2 (8)	1.1 (2)	0.24 (5)	2.9 (5)	4.4 (4)	0.21 (2)	24 (2)	6.5 (8)	1.1[a]	3.7[a]	70.54	0.91	0.15
1619-2	Liq(7)	36 (1)	0.8 (2)	0.37 (5)	2.7 (3)	7.8 (2)	0.27 (4)	25 (3)	6 (1)	0.9[a]	3.0[a]	81.68	0.85	0.14
1489	Ol(8)	41.1 (2)	0.03 (1)	0.12 (3)	-	7.0 (3)	0.15 (3)	51.3 (5)	0.12 (1)	-	-	99.15	0.93	-
1489	Opx(5)	58.0 (3)	0.06 (1)	0.35 (4)	0.8 (3)	4.5 (1)	0.15 (2)	35.0 (5)	1.1 (1)	0.3 (1)	0.11 (6)	100.25	0.93	-
1489	Grt(6)	43.3 (4)	0.43 (4)	4.6 (2)	18.5 (2)	5.7 (2)	0.28 (2)	24.1 (3)	3.4 (3)	0.09 (2)	-	100.8	0.81	0.08
1489	Liq(8)	25 (2)	1.5 (3)	0.20 (3)	2.5 (4)	7.4 (3)	0.26 (4)	20 (1)	9 (2)	1.2[a]	3.9[a]	70.47	0.83	0.20
1621-1	Ol(6)	41.7 (2)	0.02 (1)	0.08 (1)	-	5.2 (1)	0.14 (2)	52.6 (6)	0.09 (1)	-	-	99.73	0.95	-

Table 3. (continued)

Run	Phase (n)	SiO_2	TiO_2	Cr_2O_3	Al_2O_3	FeO	MnO	MgO	CaO	Na_2O	K_2O	Total	Mg#	Ca#
1621-1	Opx(5)	57.8 (2)	0.07 (1)	0.39 (15)	1.4 (2)	3.5 (1)	0.16 (2)	35.2 (2)	0.82 (5)	0.17 (1)	-	99.53	0.95	-
1621-1	Grt(7)	44.2 (2)	0.7 (1)	3.4 (6)	19.7 (2)	4.7 (1)	0.35 (2)	23.3 (4)	3.4 (3)	0.05 (1)	-	99.74	0.82	0.09
1621-1	Liq(6)	22 (2)	1.4 (3)	0.2 (1)	2.5 (5)	5.8 (6)	0.33 (2)	21 (2)	8.5 (5)	1.5[b]	4.2[b]	67.58	0.86	0.20
1501	Liq(5)	33 (2)	0.89 (8)	0.31 (4)	2.3 (6)	8.2 (8)	0.25 (6)	29 (5)	5 (2)	0.9[a]	3.2[a]	78.6	0.78	0.09
1621-2	Ol(5)	40.7 (2)	0.03 (1)	0.09 (1)	-	6.0 (1)	0.13 (2)	52.7 (2)	0.13 (1)	-	-	99.67	0.95	-
1621-2	Opx(6)	57.7 (2)	0.07 (1)	0.40 (13)	1.5 (3)	3.5 (2)	0.18 (2)	35.1 (1)	0.8 (1)	0.17 (1)	-	99.42	0.95	-
1621-2	Liq(5)	29 (3)	0.8 (2)	0.23 (3)	2.0 (3)	2.7 (1)	0.18 (2)	24 (2)	5 (1)	0.9[a]	3.5[a]	68.7	0.97	0.12
1625-1	Opx(5)	58.4 (4)	0.06 (1)	0.35 (9)	1.2 (1)	3.4 (2)	0.16 (1)	35.7 (2)	1.00 (5)	0.18 (1)	-	100.44	0.95	-
1625-1	Liq(7)	31 (1)	0.9 (1)	0.4 (1)	2.4 (2)	7 (1)	0.27 (4)	27 (1)	6 (1)	0.9[a]	3.2[a]	78.81	0.87	0.11
1495-2	Ol(7)	41.2 (3)	0.03 (1)	0.06 (2)	-	5.9 (1)	0.02 (1)	51.6 (5)	-	-	-	98.87	0.94	-
1495-2	Opx(7)	59.2 (5)	0.06 (1)	0.20 (5)	0.5 (5)	3.5 (8)	0.16 (1)	36.4 (4)	0.6 (2)	0.13 (4)	-	100.87	0.94	-
1495-2	Liq(7)	26 (1)	1.1 (2)	0.30 (3)	2.8 (2)	6.9 (4)	0.24 (3)	25 (1)	6.5 (7)	1.2[a]	3.7[a]	73.82	0.86	0.14
1625-2	Liq(6)	34 (2)	0.9 (2)	0.35 (9)	2.7 (1)	7.8 (6)	0.26 (2)	25 (1)	6.2 (1.1)	0.9[a]	3.0[a]	81.59	0.88	0.11

Notes: Numbers in parentheses are one standard deviation in terms of the last significant digit; n - number of analyses. Olivine Mg# is molar MgO/(MgO + FeO) ratio. Garnet, ortopyroxene and liquid Mg# are molar MgO /(MgO + FeO + CaO) ratios. Garnet and liquid Ca# are molar CaO/(MgO + FeO + CaO) ratios.

[a] - values corrected according to mass-balance calculations;

[b] - overestimated due to graphite-diamond conversion in the container.